Electronic Supplementary Material

Overoxidized poly(3,4-ethylenedioxythiophene)-overoxidized polypyrrole composite films with enhanced electrocatalytic ability for rutin and luteolin determination

Rongqian Meng[1,2], Jianke Tang[1,2], Hong Yang[1,2], Lijun Guo[1],Yongbo Song[1], Qiaoling Li (✉)[3], Yulan Niu (✉)[1]

1 Department of Chemistry and Chemical Engineering, Taiyuan Institute of Technology, Taiyuan 030008, China

2 School of Chemical Engineering and Technology, North University of China, Taiyuan 030051, China

3 School of Science, North University of China, Taiyuan 030051, China

E-mails: qiaolingl@163.com (Li Q); Niuyl@tit.edu.cn (Niu Y)

3.1.3 EIS analysis

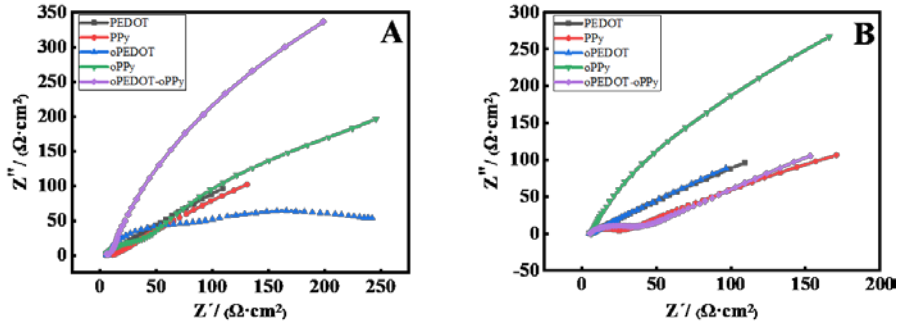

Fig. S1 Nyquist plots of various electrode materials in 5 mmol·L^{-1} $[Fe(CN)_6]^{3-/4-}$ solution with 0.1 mol·L^{-1} KCl before (A) and after incubation (B). The geometric area of the electrode : 0.07 cm^2.

3.1.4 Estimation of effective specific surface area

The chronocoulometry (CC) is used to investigate the charge (Q) - time (t) curves of PEDOT-PPy /GCE before and after incubation under different polymerization potential ranges, and the effective specific surface area (A) and electron transfer rate constant (k_s) of the electrode are calculated. The experiment is carried out in 0.1 mol L^{-1} KCl containing 1.0 mmol L^{-1} $K_3[Fe(CN)_6]$, with a potential range of 0.2~0.6 V.

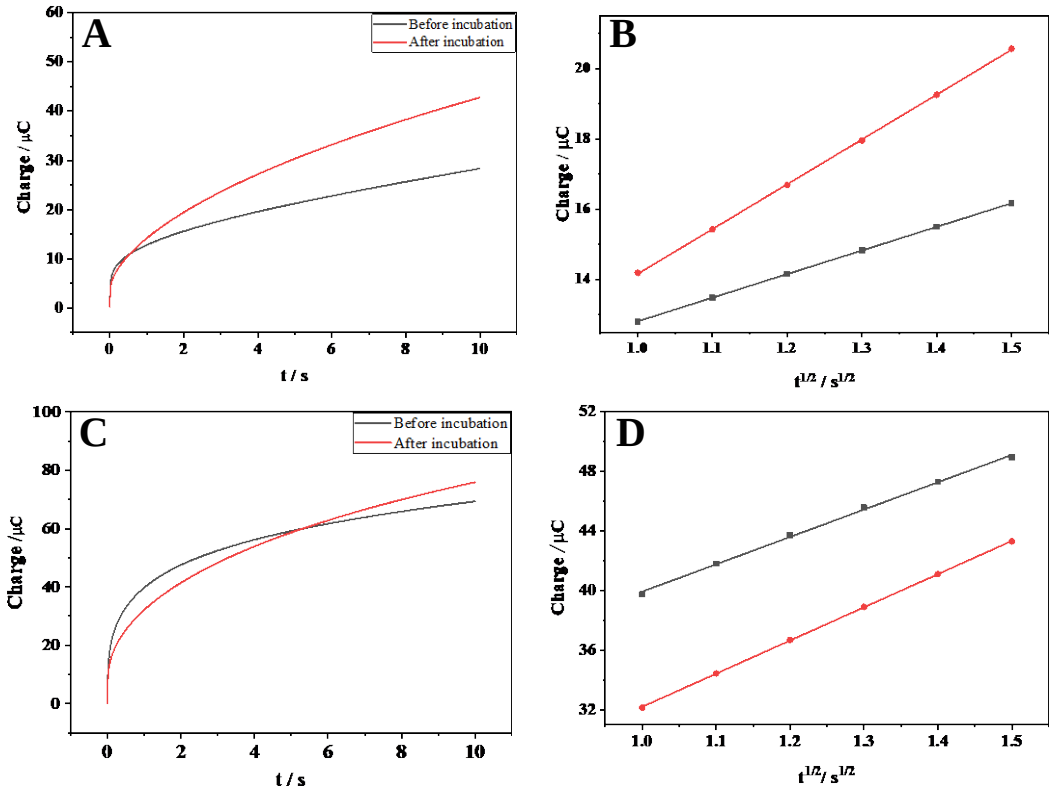

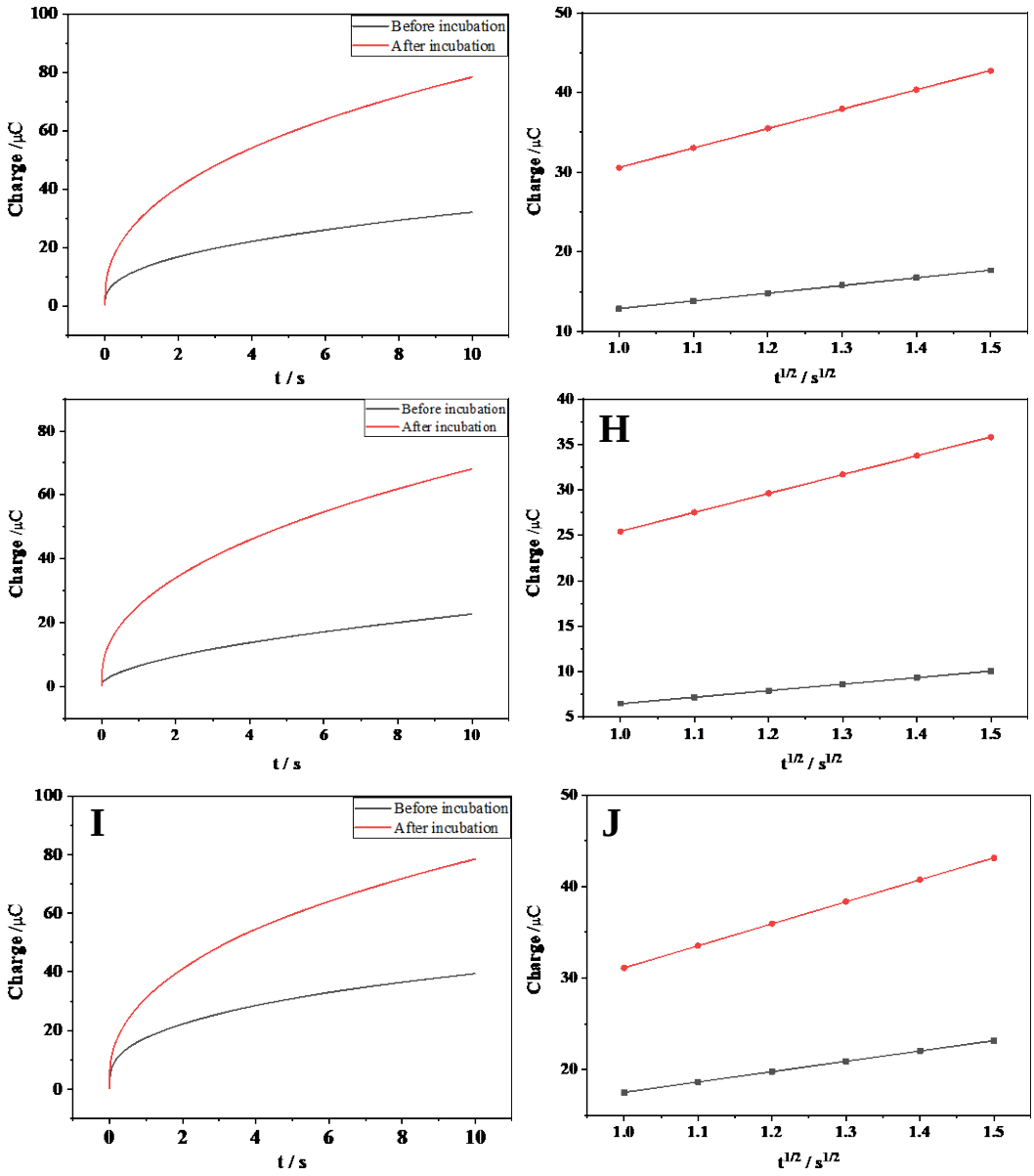

Fig. S2 Chronocoulometry of 1.0 mmol L^{-1} $K_3[Fe(CN)_6]$ solution containing 0.10 mol L^{-1} KCl determined by PEDOT-PPy/GCE determined on PEDOT-PPy/GCE prepared in the different potential range before and after incubation(left) and The linear relationship between the corresponding charge (Q) and the square root of the scan time (right), A, B: 0~0.8V; C, D: 0~1.0V; E, F: 0 ~ 1.5V; G, H: 0 ~ 1.7V; I, J: 0~1.9V

3.1.5 Estimation of standard electron-transfer rate constant

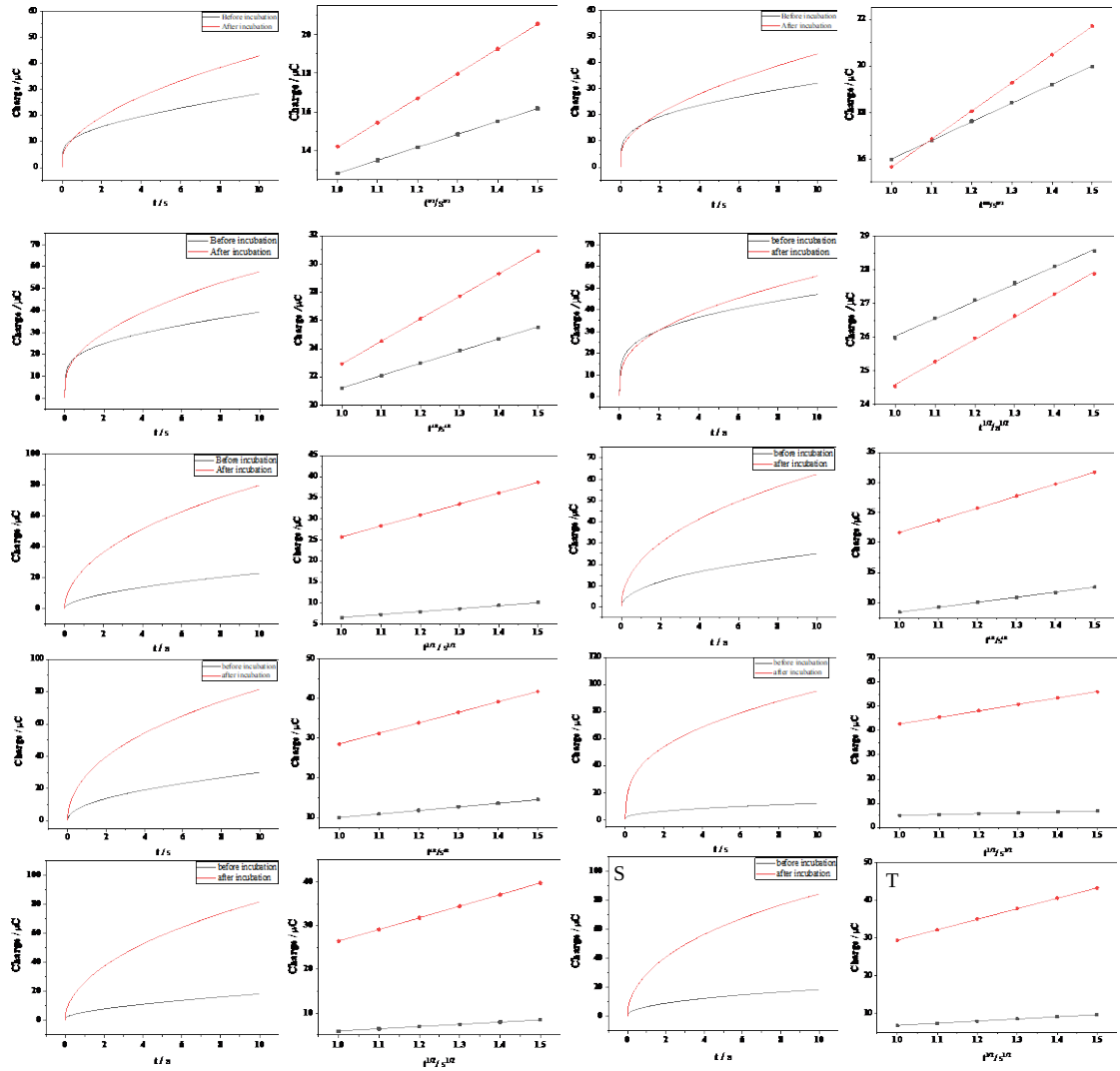

Fig. S3 Chronocoulometry of 10μmol/L rutin(the first column from the left)and 10μmol L^{-1} luteolin solution (the third column from the left) determined on PEDOT-PPy/GCE prepared in the different potential range before(black line) and after incubation(red line). The linear relationship graph between the corresponding charge (Q) and the square root of the scan time ($t^{1/2}$) for rutin (the second column from the left) and luteolin (the fourth column from left) , A-D: 0~0.8V; E-H: 0~1.0V； I-L: 0 ~ 1.5V; M-P: 0 ~ 1.7V; Q-T: 0~1.9V

3.3 Quantitative analysis of rutin and luteolin on oPEDOT-oPPy/GCE

The pH effect on the DPV peak current of rutin and luteolin at oPEDOT-oPPy/GCE was investigated in acetic acid buffer solution (ABS) with the pH ranging from 2.4 to 5.2. As shown in the Fig. 1, the current response increased with the variation in pH from 2.4 to 4.2, reached a maximum at pH 4.2, and then declined gradually. Therefore, pH 4.2 was selected as the optimum value for rutin and luteolin detection in this study.

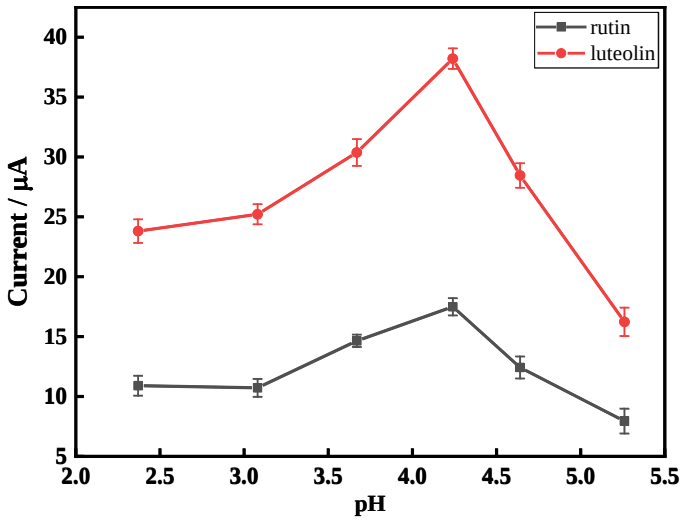

Fig. S4 Effect of pH value on the DPV peak currents of 15.0 μmol·L^{-1} rutin (black line) and luteolin (red line) at oPEDOT-oPPy/GCE, respectively

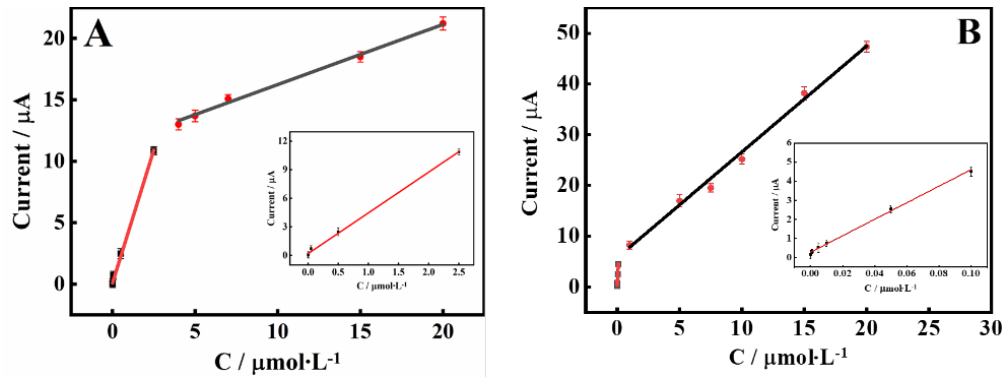

Fig. S5 Calibration curves of the concentration of rutin (A) and luteolin (B) vs. DPV peak current on oPEDOT-oPPy/GCE.

Table S1 Comparison of different modified electrodes for detection of rutin and luteolin by DPV methods.

	Modified electrode	Detection range /μmol·L^{-1}	Detection limit /nmol·L^{-1}	Ref.
Rutin	SMWCNT−PEDOT-IL Electrode	1 ~ 14	0.77	1
	GQDs/PEDOT/GCE	0.05 ~10	11	2
	MIP/G-MWCNTs/GCE	0.01–1.0	5.0	3

	oPEDOT-oPPy/GCE	0.0005 ~ 2.5 and 4 ~ 20	0.35	This work
Luteolin	MoO_3-PEDOT/CD-MOF/ GCE	0.0004 ~ 1.8	0.1	4
	PEDOT/EDTA-Ni/GCE	0.001 ~10	0.3	5
	MoO_3-PPy NWs/MWCNTs /GCE	0.0001 ~ 10.0	0.03	6
	oPEDOT-oPPy/GCE	0.0001 ~ 0.1 and 1 ~ 20	0.06	This work

The interference of metal ions during the determination of rutin and luteolin was investigated. Some possible substances are selected to estimate their effects on the DPV current response. 100-fold concentration of K^+, Zn^{2+}, Na^+, Al^{3+}, Cu^{2+}, Ba^{2+} were added to luteolin (15 μmol·L^{-1}), respectively. As shown in the Fig. S4, these additives did not interfere with the detection of rutin and luteolin since the peak current change was less than 5%. This showed that oPEDOT-oPPy/GCE has good anti-interference ability.

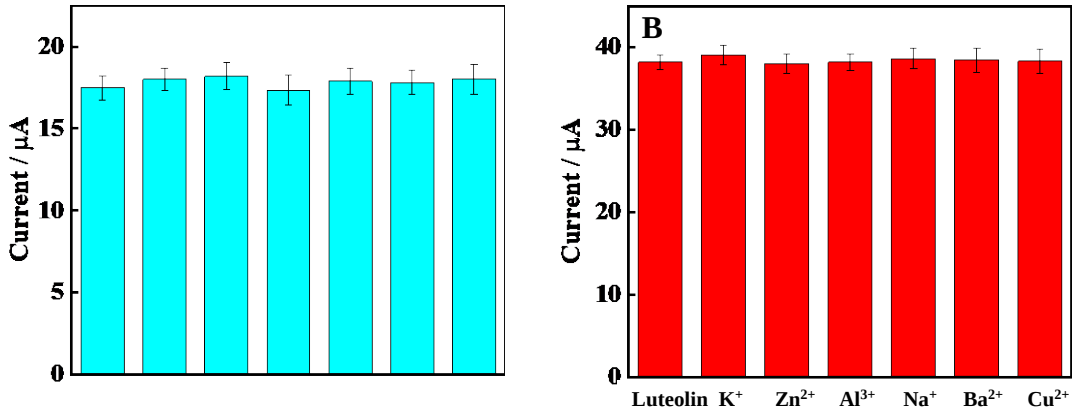

Fig. S6 Column charts of the DPV peak current of 15.0 μmol·L^{-1} rutin (A) and 15.0 μmol·L^{-1} luteolin (B) in 0.1 μmol·L^{-1} ABS solution (pH 4.2) containing 1.5 mmol·L^{-1} metal ions

3.5.1 XPS analysis

Table S2 Binding energy and contents of each component in the O1s spectrum of oPEDOT-oPPy film incubated for different times

time/min	$-SO_2/-SO$		-C=O/-O-C=O		-C-O-C-		-COOH	
	BE/eV	%	BE/eV	%	BE/eV	%	BE/eV	%
0	530.6	1.5	531.7	24.3	532.9	73.5	535.7	0.7
10	530.6	22.4	531.4	29.5	532.5	39.4	535.5	8.7
20	530.7	22.8	531.5	30.1	532.7	40.7	535.4	6.5
30	530.7	23.9	531.4	29.5	532.7	39.8	535.5	6.7

Table S3 Binding energy and contents of each component in the N1s spectrum of oPEDOT-oPPy film incubated for different times

time/min	-C-N=/-C=N-		-NH-		$-C-N^+-$		$-C=N^+-$	
	BE/eV	%	BE/eV	%	BE/eV	%	BE/eV	%
0	398.3	4.42	400.1	88.5	401.5	3.5	402.5	3.5
10	398.2	21.6	399.8	74.6	401.1	1.5	402.2	2.2
20	398.3	23.4	399.9	73.0	401.2	2.9	402.6	0.7
30	398.3	24.4	399.9	74.1	----	----	402.5	1.5

Table S4 Binding energy and contents of each component in the S2p spectrum of oPEDOT-oPPy film incubated for different times

time/min	S2p3/2		S2p1/2		S^+		$-SO_2/-SO$	
	BE/eV	%	BE/eV	%	BE/eV	%	BE/eV	%
0	163.8	44.4	164.9	28.4	166.1	5.8	168.4/169.6	21.3
10	163.8	39.1	164.9	21.1	166.5	5.1	168.1/169.2	34.8
20	163.9	50.0	165.2	13.5	166.5	5.5	168.2/169.5	31.0
30	163.8	44.1	165.1	23.8	166.3	3.5	168.1/169.2	28.6

3.5.2 Raman and FT-IR spectroscopy analysis

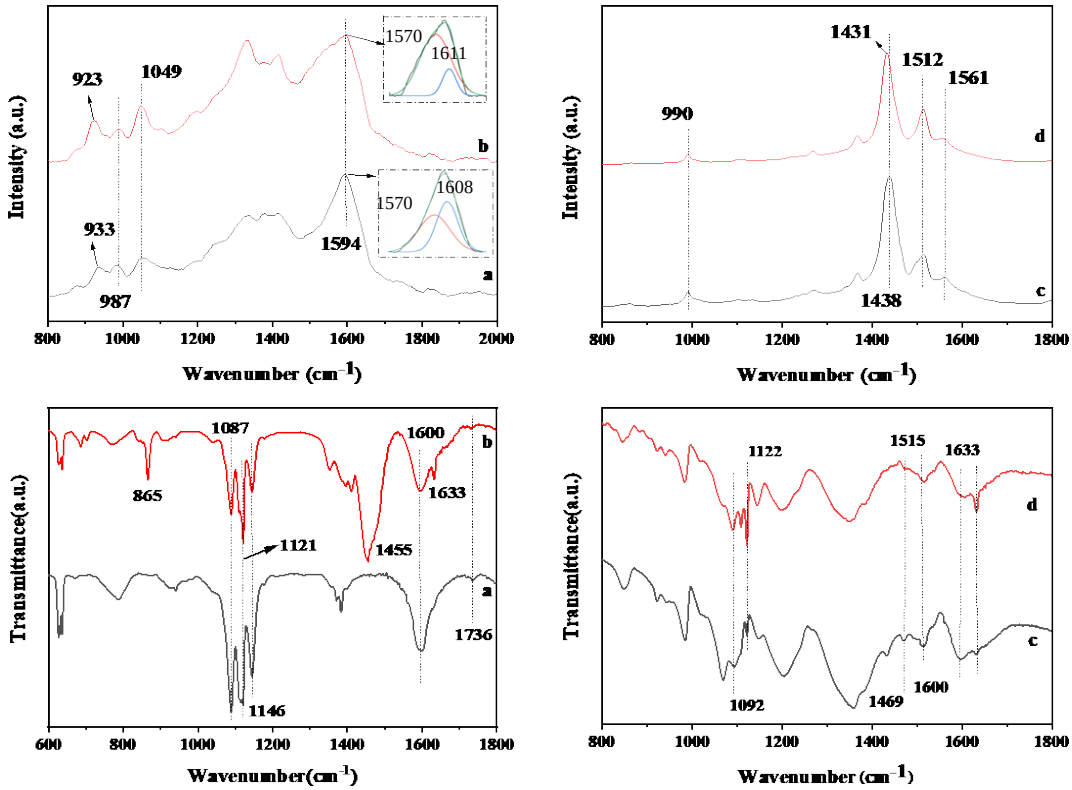

Fig. S7 Raman spectrum (A and B) and FTIR Spectrum (C and D) analysis of single films before (black line) and after(red line) incubation . A and C: OPPy; B and D: OPEDOT films.（The excitation laser of Raman spectrum is 514nm）

Fig. S7-A showed the Raman spectra before (a) and after (b) incubation OPPy incubation. The absorption peak at 1594 cm^{-1} corresponded to the skeleton stretching vibration peak of the pyrrole ring -C=C- bond. This broad peak can be fitted into two Lorentzian peaks [7]. One was at 1570 cm^{-1} and the other was at 1608 (1611) cm^{-1} as shown in the Fig. S3-A , which was assigned to the benzene-type (reduced) and quinone type (oxidized) pyrrole ring, respectively [8]. The peak area ratios of benzene-type and quinone-type (I_{1570}/I_{1603} and I_{1570}/I_{1611}) before and after incubation were 1.08 and 5.25, respectively, indicating that the peak area of benzene-type pyrrole structure in OPPy increased obviously after incubation, resulting in enhanced conjugation [9]. Absorption peaks at 1049, 987 and 923/933cm^{-1} corresponded to -C-H- in-plane, pyrrole ring deformation vibration caused by polaron, and -C-H- out-of-plane deformation vibration caused by bipolaron [8], respectively. The peak strength ratios before and after incubation(I_{933}/I_{987} and I_{923}/I_{987}) were calculated to 1.2 and 2.25, respectively, which increased by nearly two times. That is, after incubation, more N^+ existed in the form of bipolarons, and more -C=N- bonds were formed.

Fig. S7-B showed the Raman spectra of OPEDOT before (c) and after (d) incubation. The main characteristic peaks of OPEDOT films were assigned as follows: 1438/1431 cm^{-1} (C_α=C_β symmetric stretching vibration), 1512 /1561 cm^{-1}(C_α=C_β antisymmetric stretching vibration), and 1368cm^{-1} (C_β-$C_{\beta'}$stretching vibration), 1260cm^{-1}(intra-ring stretching vibration of C_α-$C_{\alpha'}$), and 990 cm^{-1}(C-C anti-symmetric stretching vibration)[9-10]. It was observed that the symmetrical stretching peak of C_α=C_β shifted from 1438 to 1431cm^{-1} after incubation, and the half-peak width was narrowed indicating that the conjugated structure of thiophene ring changed from benzene

type to quinone type [10], which was conducive to the transfer of π electrons on polymerization chains [11].

Fig. S7-C showed the FT-IR spectra of OPPy before (a) and after incubation (b). Absorption peaks appeared at 1736, 1600, 1146, 1087 cm^{-1}, corresponding to -C=O, -C=C-, -C-C-, -O-H/ -C-O stretching vibration [12-14], respectively. The -C=O absorption peak indicated that overoxidation occurs in pyrrole before and after incubation. The peak of -C=N- structure appeared at 1633 cm^{-1} after incubation, which may be due to the dissociation of H atom on -NH-in pyrrole ring under alkaline incubation conditions, resulting in the formation of -C=N- bonds [14].

Fig. S7-D showed the FT-IR spectra of OPEDOT before (c) and after (d) incubation. The absorption peaks were assigned as follow: 846/941 cm^{-1} (-C-S- stretching vibration), 1066/1146/1203 cm^{-1} (-C-O-C- stretching vibration), 1092/1122 cm^{-1} (-SO_2/-SO stretching vibration) , 1350 cm^{-1} (-C-C- stretching vibration), respectively [15-16]. The peaks at 1431,1469 and 1600 cm^{-1} corresponded to -C_α=C_β- of benzene-type structure in thiophene ring[17], while the peaks at 1515, 1633 cm^{-1} corresponded to C_α=C_β of quinone-type structure in thiophene ring[18-19]. After incubation, the peak intensity (I) at 1633 and 1515 cm^{-1} increased significantly compared with that at 1600 cm^{-1}. By calculating the absorption peak intensity ratio of -C=C- bond from benzene-type and quinone-type structure, the value of I_{1600} / I_{1633} and I_{1469} / I_{1515} were 1.20 and 0.60 before incubation, which were 0.72 and 0.43 after incubation, respectively, indicating that the benzene-type structure was weakened while quinone-type structure was enhanced. The results showed that PEDOT polymer changed from benzene-type to quinone-type structure after incubation, which was consistent with Raman results.

3.6 Electrocatalytic mechanism of oPEDOT-oPPy composite films

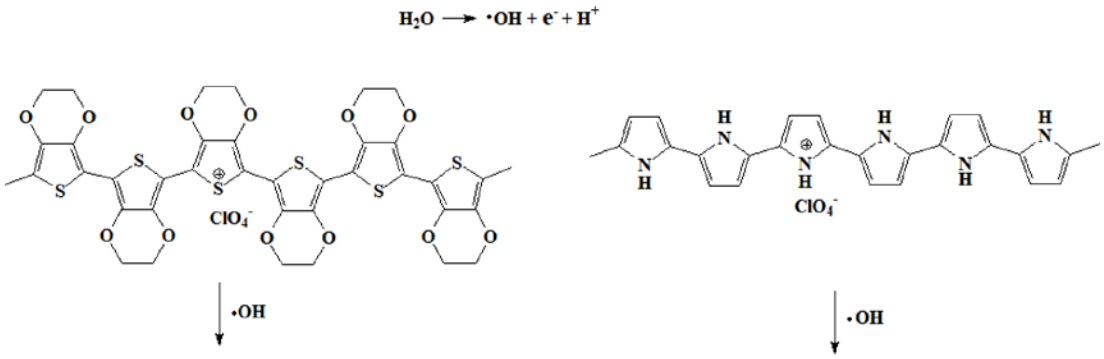

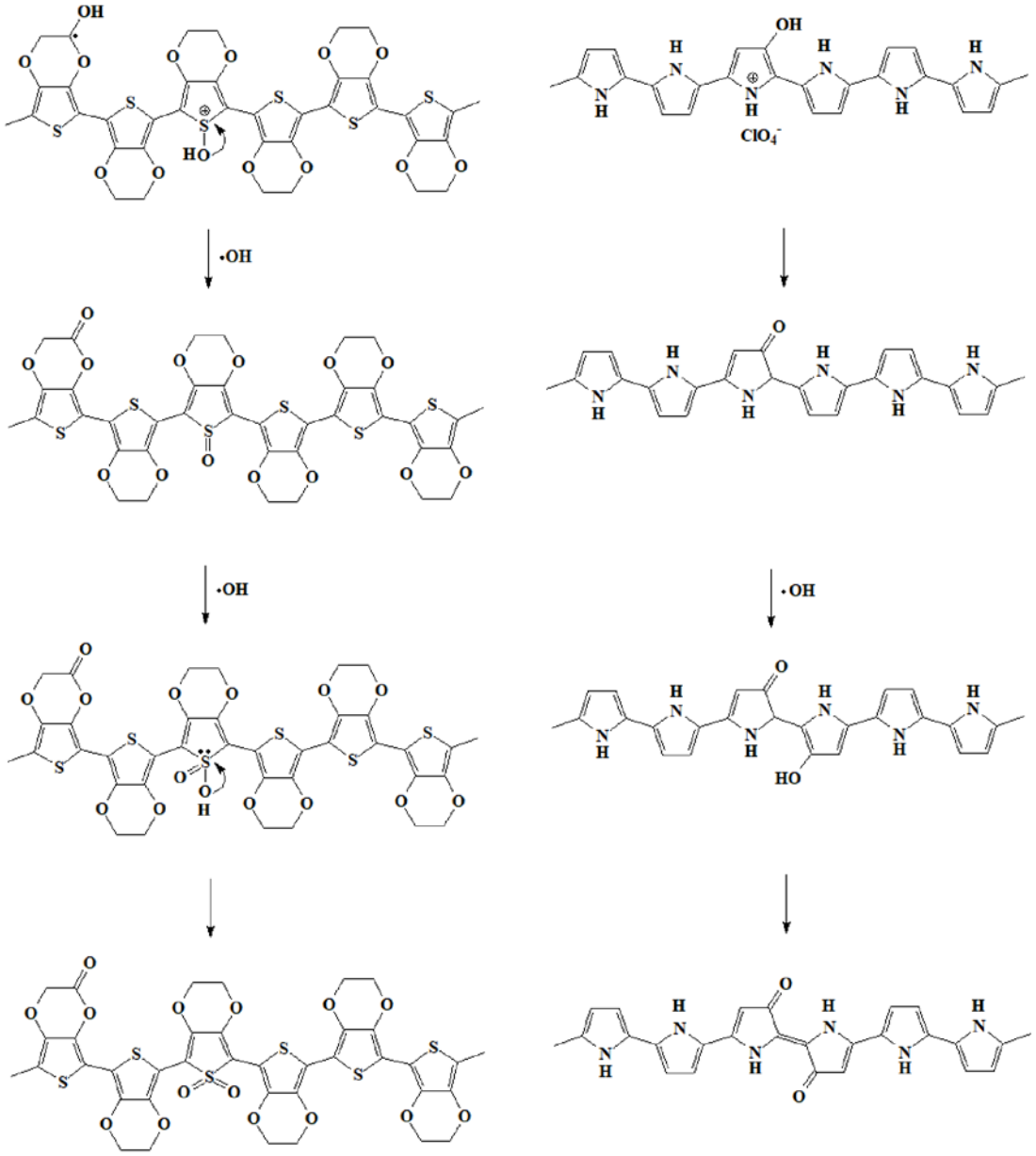

Fig. S8 Proposed overoxidation mechanism of oPEDOT and oPPy in composite film prepared at the high potential [20-21].

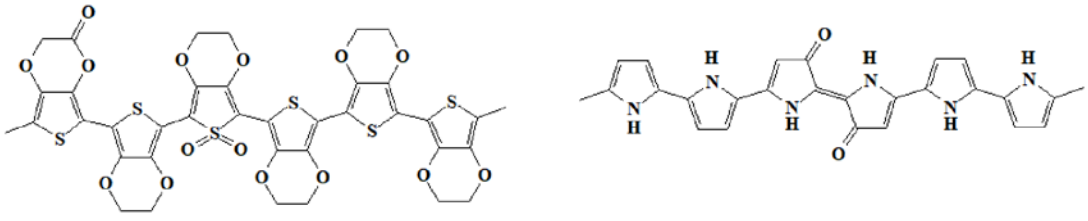

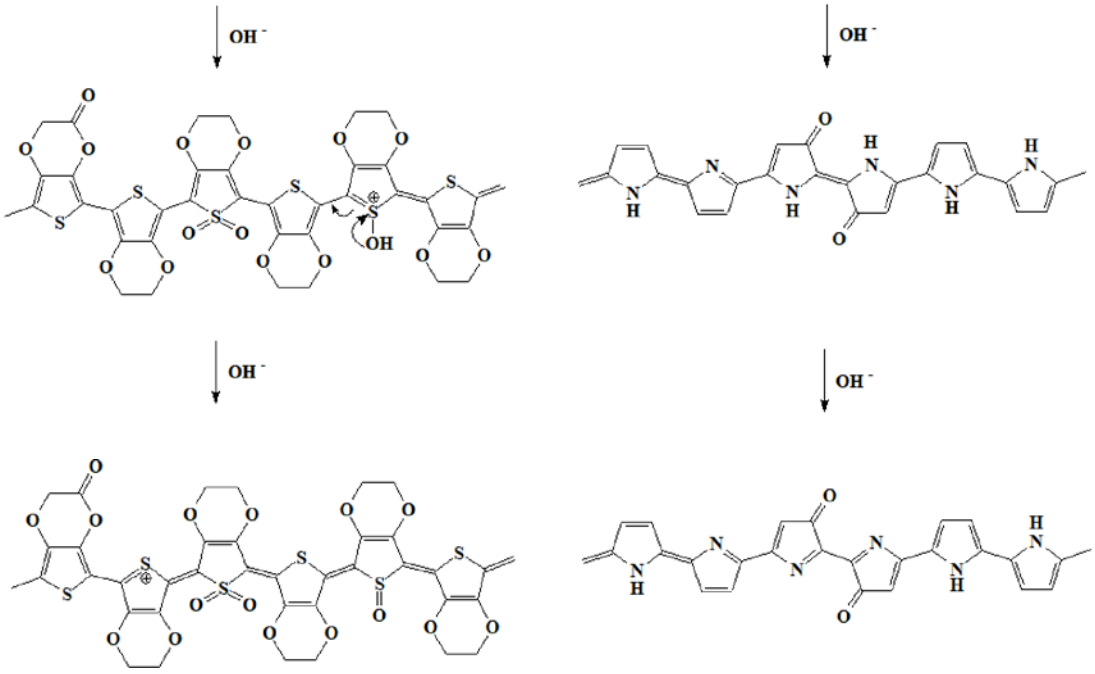

Fig. S9 Proposed incubation mechanism for oPEDOT and oPPy in composite film after incubation in NaOH-EtOH solution.

3.7.1 Frontier molecular orbital analysis

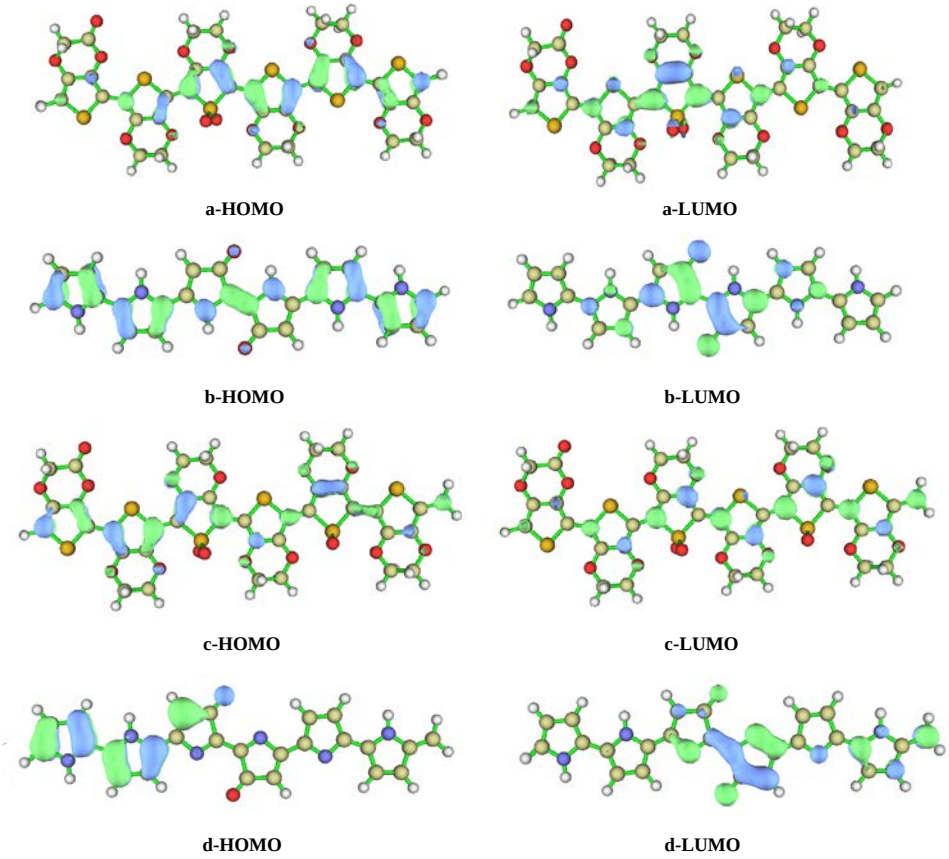

Fig. S10 Spatial distribution of the frontier molecular orbitals of $oPEDOT_6$ (a, c) and $oPPy_6$(b, d)

before and after incubation.

3.7.2 Adsorption energy analysis

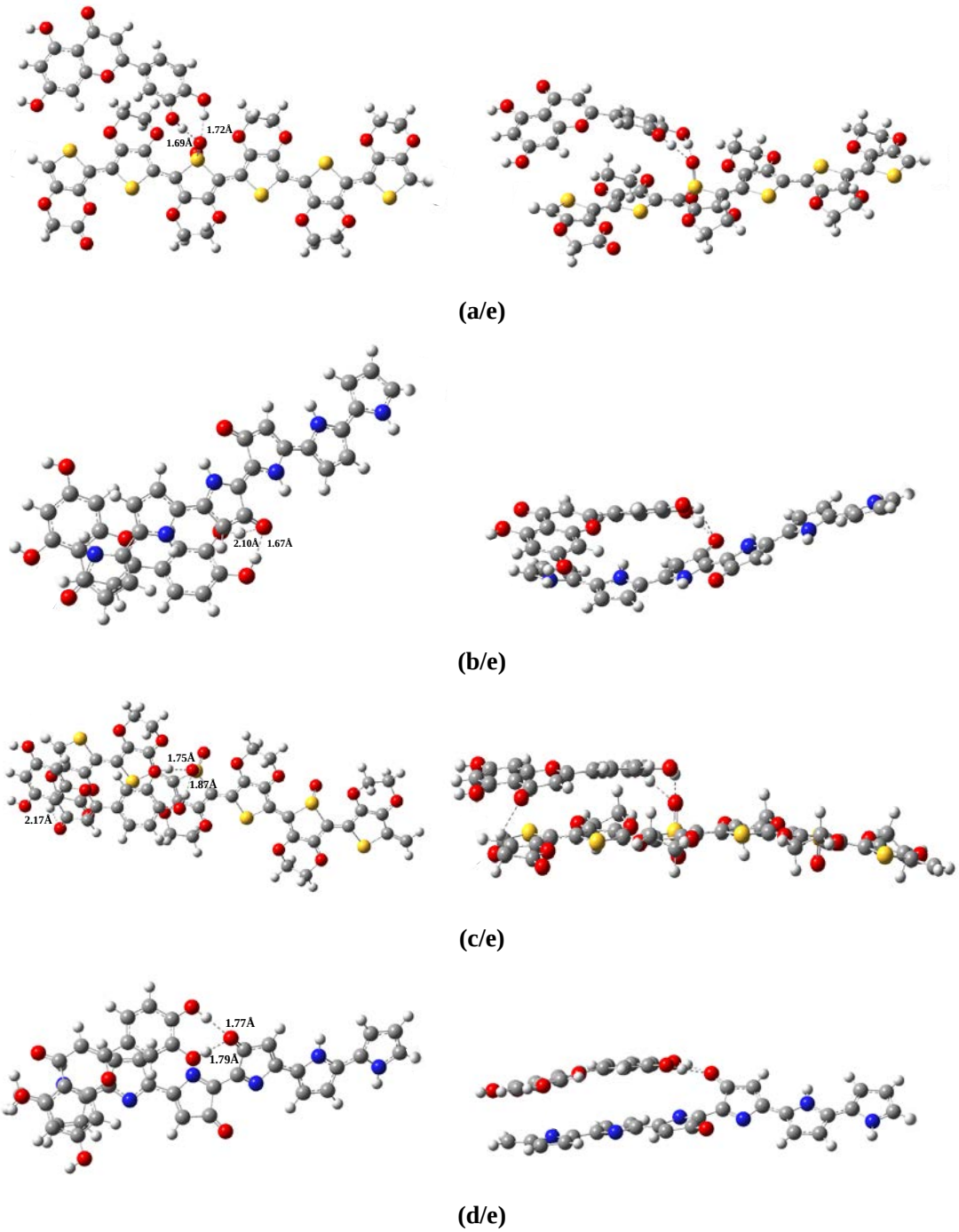

Fig. S11. Front view (left) and side view (right) of optimal geometry of oPEDOT$_6$(a, c)and oPPy$_6$ (b, d) before and after incubation complex with luteolin (e) (a/e, b/e, c/e and d/e).

Reference

1. Nagles E, García-Beltrán O. Determination of Rutin in Black Tea by Adsorption

Voltammetry (AdV) in the Presence of Morin and Quercetin. Food Analytical Methods, 2016, 9 (12): 3420-3427

2. Meng R Q L, Q L，Zhang S J, Tang J K， Ma C L，Jin R Y. GQDs/PEDOT Bilayer Films Modified Electrode as a Novel Electrochemical Sensing Platform for Rutin Detection. International Journal of Electrochemical Science, 2019, 14(12): 11000-11011
3. Yang L T, Yang J, Xu B J, Zhao F Q, Zeng B Z. Facile preparation of molecularly imprinted polypyrrole-graphene-multiwalled carbon nanotubes composite film modified electrode for rutin sensing. Talanta, 2016, 161: 413-418
4. Chen X, Li J D, Li J, Zhang L, Zhao P C, Wang C X, Fei J J, Xie Y X. Determination of luteolin in Chrysanthemum tea with a ultra-sensitive electrochemical sensor based on MoO_3/poly(3,4-ethylene dioxythiophene)/gama-cyclodextrin metal-organic framework composites. Food Chemistry, 2022, 397: 133723-133730
5. Wu L P, Gao Y S, Xu J K, Lu L M, Nie T. Novel Nickel Redox Polymer as an Efficient Electrode Material for Electrochemical Sensing. Electroanalysis, 2014, 26 (10): 2207-2215
6. Zeng Q, Chen J F, Gao F, Tu X L, Qian Y , Yu Y F, Lu L M, Wang W M. Development of a new electrochemical sensing platform based on MoO3-polypyrrole nanowires/MWCNTs composite and its application to luteolin detection. Synthetic Metals, 2021, 271: 116620-116627
7. Chen F, Shi G Q, Fu M X, Qu L T, Hong X Y. Raman spectroscopic evidence of thickness dependence of the doping level of electrochemically deposited polypyrrole film. Synthetic Metals, 2003, 132: 125-132
8. Santos M J L, Brolo A G, Girotto E M. Study of polaron and bipolaron states in polypyrrole by in situ Raman spectroelectrochemistry. Electrochimica Acta, 2007, 52: 6141–6145
9. Kulandaivalu S, Zainal Z, Sulaiman Y. Influence of Monomer Concentration on the Morphologies and Electrochemical Properties of PEDOT, PANI, and PPy Prepared from Aqueous Solution. International Journal of Polymer Science,

2016, 2016: 1-10

10. Culebras M, Gómez C M, Cantarero A. Enhanced thermoelectric performance of PEDOT with different counter-ions optimized by chemical reduction. Journal of Materials Chemistry A, 2014, 2: 10109-10115
11. Ouyang J Y, Xu Q F, Chu C W, Yang Y, Li G, Shinar J. On the mechanism of conductivity enhancement in poly(3,4-ethylenedioxythiophene):poly(styrene sulfonate) film through solvent treatment. Polymer, 2004, 45: 8443-8450
12. Radhakrishnan S, Sumathi C, Umar A, Kim S J, Wilson J, Dharuman V. Polypyrrole-poly(3,4-ethylenedioxythiophene)-Ag (PPy-PEDOT-Ag) nanocomposite films for label-free electrochemical DNA sensing. Biosensors and Bioelectronics, 2013, 47: 133-140
13. Yalçınkaya S, Demetgül C, Timur M, Çolak N. Electrochemical synthesis and characterization of polypyrrole/chitosan composite on platinum electrode: Its electrochemical and thermal behaviors. Carbohydrate Polymers, 2010, 79: 908-913
14. Mathys G I, Truong V T. Spectroscopic study of thermo-oxidative degradation of polypyrrole powder by FT-IR. Synthetic Metals, 1997, 89: 103-109
15. Chen T, Qiu J H, Zhu K J, Li J H, Wang J W, Li S Q, Wang X L. Ultra high permittivity and significantly enhanced electric field induced strain in PEDOT:PSS–RGO@PU intelligent shape-changing electro-active polymers. RSC Advance, 2014, 109: 64061-64066
16. Han Y Q, Shen M X, Wu Y, Zhu J J, Ding B, Tong H, Zhang X G. Preparation and electrochemical performances of PEDOT/sulfonic acid-functionalized graphene composite hydrogel. Synthetic Metals, 2013, 172: 21-27
17. Leš K, Jordan C S. Ionic conductivity enhancement in solid polymer electrolytes by electrochemical in situ formation of an interpenetrating network. RSC Advances, 2020, 10: 41296-41303
18. Song J C, Noh H J, Lee J H, Nah I W, Cho W I, Kim H T. In situ coating of Poly(3,4-ethylenedioxythiophene) on sulfur cathode for high performance lithium–sulfur batteries. Journal of Power Sources, 2016, 332: 72-78

19. Chen H W, Dong W L, Ge J, Wang Ch H, Wu X D, Lu W, Chen L W. Ultrafine sulfur nanoparticles in conducting polymer shell as cathode materials for high performance lithium/sulfur batteries. Scientific Reports, 2013, 3: 1910-1915
20. Láng G G, Ujvári M, Vesztergom S, Kondratiev V, Gubicza J, Szekeres K J. The Electrochemical Degradation of Poly(3,4-ethylenedioxythiophene) Films Electrodeposited from Aqueous Solution. Zeitschrift für Physikalische Chemie, 2016, 230: 1281-1286
21. Ge H L, Qi G J, Kang E T, Neoh K G. Study of overoxidized polypyrrole using X-ray photoelectron spectroscopy. Polymer, 1994, 35: 504-508